magnetochemistry

MDPI

Article

A Spin Crossover Transition in a Mn(II) Chain Compound

Samia Benmansour [1], Smail Triki [2] and Carlos J. Gómez-García [1,*]

Received: 1 December 2015; Accepted: 21 December 2015; Published: 29 December 2015
Academic Editor: Melanie Pilkington

[1] Instituto de Ciencia Molecular (ICMol), Universidad de Valencia, C/ Catedrático José Beltrán 2, 46980 Paterna, Valencia, Spain; sam.ben@uv.es
[2] UMR CNRS 6521, Chimie, Electrochimie Moléculaires, Chimie Analytique, Université de Bretagne Occidentale, BP 809, 29285 Brest Cedex, France; smail.triki@univ-brest.fr
* Correspondence: carlos.gomez@uv.es; Tel.: +34-963544423; Fax: +34-963543273

Abstract: Three new compounds have been synthesized and characterized with Fe(II), Co(II) and Mn(II), the polynitrile anionic ligand 1,1,3,3-tetracyano-2-(3-hydroxypropoxy)-propenide (tcnopr3OH$^-$) and the co-ligand 4,4′-bipyridine (4,4′-bpy). The Fe(II) compound, formulated as [Fe^{II}(tcnoprOH)$_2$(H$_2$O)$_2$(4,4′-bpy)$_2$] (**1**), contains monomeric complexes where the Fe(II) ion is coordinated to two *trans* polynitrile ligands, two *trans* 4,4′-bpy ligands and two *trans* water molecules. Compounds [M^{II}(H$_2$O)$_4$(μ-4,4′-bpy)][M^{II}(tcnoprOH)$_4$(μ-4,4′-bpy)].3H$_2$O, M = Mn (**2**) and Co (**3**), are isostructural and crystallize in segregated cationic and anionic chains that can be formulated as [M^{II}(H$_2$O)$_4$(μ-4,4′-bpy)]$_n^{2n+}$ and [M^{II}(tcnoprOH)$_4$(μ-4,4′-bpy)]$_n^{2n-}$, respectively with M = Mn (**2**) and Co (**3**). The magnetic properties of Compound **1** show the expected paramagnetic behavior for an isolated high spin S = 2 Fe(II) ion with a zero field splitting of $|D| = 4.0(1)$ cm^{-1}. Compound **3** presents the expected behavior for isolated Co(II) centers, whereas Compound **2** shows an unexpected partial smooth spin crossover (SCO) transition in the anionic [Mn^{II}(tcnoprOH)$_4$(μ-4,4′-bpy)]$_n^{2n-}$ chain together with a paramagnetic contribution of the cationic [Mn^{II}(H$_2$O)$_4$(μ-4,4′-bpy)]$_n^{2n+}$ chain. This behavior has been confirmed with DSC measurements. This is one of the very few examples of SCO transition observed in a Mn(II) complex and the first one in a Mn(II) chain.

Keywords: Mn(II) spin crossover; low spin Mn(II); chain compounds; magnetic coordination polymers; polynitrile ligands

1. Introduction

The synthesis of new coordination polymers (CP) with interesting properties constitutes a hot topic given the interesting properties that these materials may show. Thus, although many CP have been synthesized with different magnetic [1–3], electrical [4] and/or optical properties [5,6], the design and preparation of novel CP with tailored properties remains a challenge. The most used strategies to reach this goal are: (i) the use of simple bridging ligands, such as azide (N_3^-) [7–11], cyanide (CN^-) [12] dicyanamide ($N(CN)_2^-$) [13–15], oxalato ($C_2O_4^{2-}$), ... [16], combined with different transition metal atoms; (ii) the use of metalloligands [17–19], *i.e.*, pre-formed metal complexes able to coordinate to other metal atoms; and (iii) the use of bridging ligands and co-ligands with different metal atoms in order to obtain CP with alternating ligands or metals. Besides the aforementioned simple bridging ligands, other, more complex poly-dentate bridging ligands and co-ligands, such as polynitrile anions, have also been used to prepare many different CP [20–26].

In this context, in previous works with polynitrile anions, we have synthesized different ligands with up to four cyano groups oriented in two different directions and an additional potentially coordinating alcohol or thiol function (Scheme 1) [27].

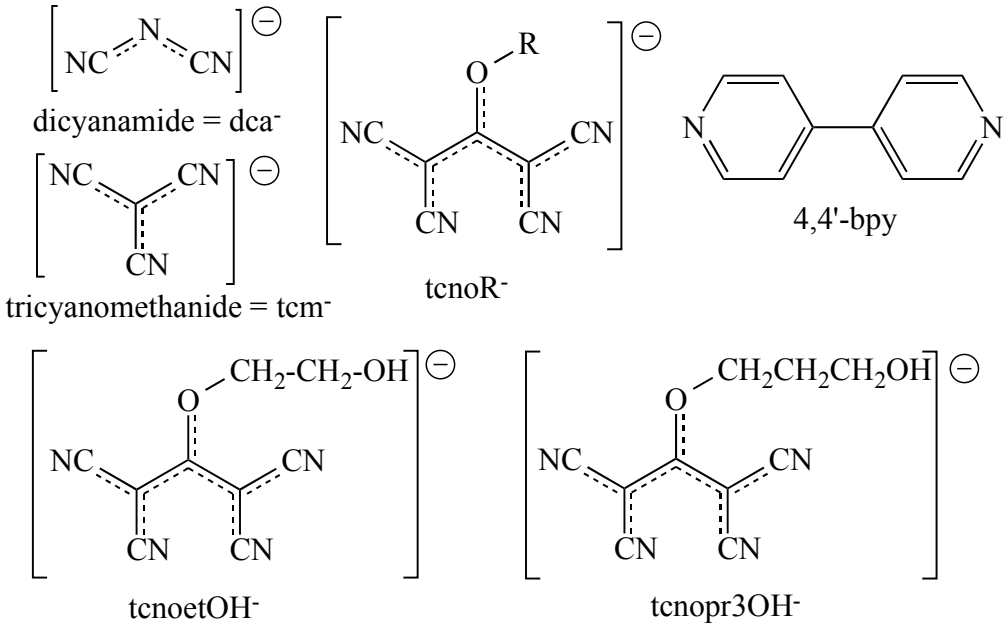

Scheme 1. Some ligands used to prepare coordination polymers (CP), including the ligands used in this work. bpy, bipyridine; tcnopr3OH$^-$, 1,1,3,3-tetracyano-2-(3-hydroxypropoxy)-propenide.

Among the polynitrile ligands used to prepare coordination polymers (Scheme 1), the most versatile one has been tcnopr3OH$^-$ (1,1,3,3-tetracyano-2-(3-hydroxypropoxy)-propenide), thanks to the presence of a longer and, therefore, more flexible alkyl chain. Thus, the combination of this ligand with different transition metals yielded two closely-related series of CP, formulated as [*M*(1k*N*:2k*O*-tcnopr3OH)$_2$(H$_2$O)$_2$] (M^{II} = Mn, Fe, Co, Ni, Cu and Zn) and [*M*(1k*N*:2k*N*′-tcnopr3OH)$_2$(H$_2$O)$_2$] (M^{II} = Fe, Co and Ni) [22,28]. Interestingly, three metal ions (Fe, Co and Ni) gave rise to both linkage isomers and constitute the first series of CP presenting linkage isomerism [28].

Additionally, in a previous work, we have shown that the closely-related polynitrile ligand 1,1,3,3-tetracyano-2-(2-hydroxyethoxy)-propenide (tcnoetOH$^-$; Scheme 1) can be combined with a bridging co-ligand as 4,4′-bipyridine (4,4′-bpy; Scheme 1) to prepare one-dimensional coordination polymers with Fe(II), Co(II) and Ni(II) [29]. In these CP, the metal ions are connected by 4,4′-bpy bridges located in *trans* to form regular linear chains. The metal ions complete their octahedral coordination geometries with two *trans* water molecules and two *trans* polynitrile ligands.

In the present work, we will combine both strategies in order to prepare new CP with magnetic properties. Thus, we will explore the effect of extending the alkyl chain in the polynitrile ligand by including an extra carbon atom (*i.e.*, with a –prOH arm instead of –etOH) and the effect of the presence of a bridging co-ligand as 4,4′-bpy. Thus, here, we present the results obtained with the polynitrile anion 1,1,3,3-tetracyano-2-(3-hydroxypropoxy)-propenide (tcnopr3OH$^-$) and 4,4′-bipyridine (4,4′-bpy) as a bridging co-ligand combined with different transition metal ions as Mn(II), Fe(II) and Co(II). This study shows that both the additional carbon atom in the side chain of the polynitrile ligand and the transition metal ion play a key role in the final structure obtained. Thus, Fe(II) forms a centro-symmetric monomer formulated as [Fe^{II}(tcnopr3OH)$_2$(H$_2$O)$_2$(4,4′-bpy)$_2$] (**1**) with two *trans* (tcnopr3OH)$^-$ ligands, two *trans* 4,4′-bpy ligands and two *trans* water molecules. In contrast, Mn(II) and Co(II) form two isostructural coordination polymers formulated as [M^{II}(H$_2$O)$_4$(μ-4,4′-bpy)][M^{II}(tcnoprOH)$_4$(μ-4,4′-bpy)]· 3H$_2$O with *M* = Mn (**2**) and Co (**3**). These CP present segregated cationic and anionic chains formulated as [M^{II}(H$_2$O)$_4$(μ-4,4′-bpy)]$^{2+}$ and [M^{II}(tcnoprOH)$_4$(μ-4,4′-bpy)]$^{2-}$. We also present here the magnetic characterization of the three compounds. Compounds **1** and **3** show the expected paramagnetic behavior for high spin Fe(II) and Co(II) ions, whereas the Mn(II) compound presents a very unusual

partial spin crossover transition in the anionic Mn(II) chain coexisting with the high spin Mn(II) cationic chain. Compound **2** is, therefore, one of the very scarce examples of spin crossover transitions in a Mn(II) complex and the first one with the coexistence of smooth spin crossover (SCO) and high spin Mn(II) ions.

2. Results and Discussion

2.1. Syntheses and Spectroscopic Characterizations of the Complexes

The synthesis of the three compounds was performed under similar conditions and using a method similar to that used to prepare the closely-related compounds with the ligand tcnoetOH$^-$ (Scheme 1). Unexpectedly, the Fe(II) ion crystallized as a monomer surrounded by two *trans* tcnopr3OH$^-$ ligands, two *trans* water molecules and two *trans* terminal 4,4′-bpy molecules. In contrast, Mn(II) and Co(II) ions crystallize forming segregated linear cationic and anionic chains with *trans* bridging 4,4′-bpy ligands and four tcnopr3OH$^-$ ligands (anionic chains) or four water molecules (cationic chains) completing the octahedral coordination of the metal ions. Of course, we cannot attribute these different behaviors to the metal ion size, since the ionic radius of Fe(II) is intermediate between Mn(II) and Co(II). Furthermore, when using the closely-related tcnoetOH$^-$ ligand with Fe(II), Co(II) and Ni(II), the obtained compounds present linear neutral chains containing the metal ions coordinated to two *trans* tcnoetOH$^-$ ligands, two *trans* water molecules and two *trans* 4,4′-bpy ligands [29] (*i.e.*, the metal ions have the same coordination environmentthan Fe(II) in Compound **1**, but with bridging 4,4′-bpy molecules instead of terminal ones, as in (**1**).

The IR spectra of the three complexes are very similar: they show doublets at 2245/2210, 2237/2206 and 2238/2207 cm^{-1} in **1**–**3**, respectively, corresponding to the coordinated and non-coordinated cyano groups, respectively. A broad band at *ca.* 3400 cm^{-1} confirms the presence of water molecules in the three compounds.

2.2. Description of the Structures

Structure of [Fe^{II}(tcnoprOH)$_2$(4,4′-bpy)$_2$(H$_2$O)$_2$] (**1**): Compound **1** crystallizes in the triclinic space group P-*1* and is formed by isolated monomeric Fe(II) complexes. The asymmetric unit of **1** contains a Fe(II) ion located in a special position (1/2, 1/2, 1/2), one tcnopr3OH$^-$ anion, one 4,4′-bpy ligand and one water molecule, all located in general positions. This asymmetric unit generates an isolated centro-symmetric complex with two terminal tcnopr3OH$^-$ ligands, two terminal 4,4′-bpy ligands and two water molecules (Figure 1). The inversion center located on the Fe(II) ion generates a *trans* disposition of each couple of ligands. The bond lengths and angles (Table 1) show that the coordination geometry around the Fe(II) ion is a quite regular octahedron of the type of N$_4$O$_2$ containing two N atoms from two 4,4′-bpy molecules (N5 and N5*), two N atoms from the tcnopr3OH$^-$ ligands (N1 and N1*) and two oxygen atoms from two water molecules (O1 and O1*) (Figure 1). The molecules are isolated and are only connected by π-π interactions established between the aromatic rings of the 4,4′-bpy molecules. These interactions give rise to stacks of molecules along the *a* direction (Figure 2) with two different short average inter-plane distances of 3.37 and 3.48 Å. These π-π interactions may be the reason for the longer Fe–N$_{bpy}$ bond distance compared to the Fe–N$_{tcnoprOH}$ one (2.212(16) *vs.* 2.182(2) Å).

Structure of [*M*(H$_2$O)$_4$(μ-4,4′-bpy)][*M*(tcnoprOH)$_4$(μ-4,4′-bpy)].3H$_2$O, *M*^{II} = Mn (**2**) and Co (**3**): Compounds **2** and **3** are isostructural and crystallize in the monoclinic space group P*2/n*. The asymmetric unit contains two independent metal ions, two tcnopr3OH$^-$ ligands, two water molecules and two 4,4′-bpt bridging ligands. Each independent metal ion (*M*1 and *M*2) forms a different linear chain, although with identical bridges. Thus, in both chains, the metal ions are connected through two *trans* 4,4′-bpy bridging ligands (Figure 3). The differences between both chains consist in the ligands located perpendicular to the chain direction: four tcnopr3OH$^-$ ligands for *M*1 and four H$_2$O molecules for *M*2. This different ligand distribution gives rise to different charges in the chains. Thus, the chain

formulated as $[M(H_2O)_4(\mu\text{-}4,4'\text{-bpy})]^{2+}$ is cationic and bears a +2 charge per metal ion, whereas the chain formulated $[M(\text{tcnoprOH})_4(\mu\text{-}4,4'\text{-bpy})]^{2-}$ bears a charge of −2 per metal ion.

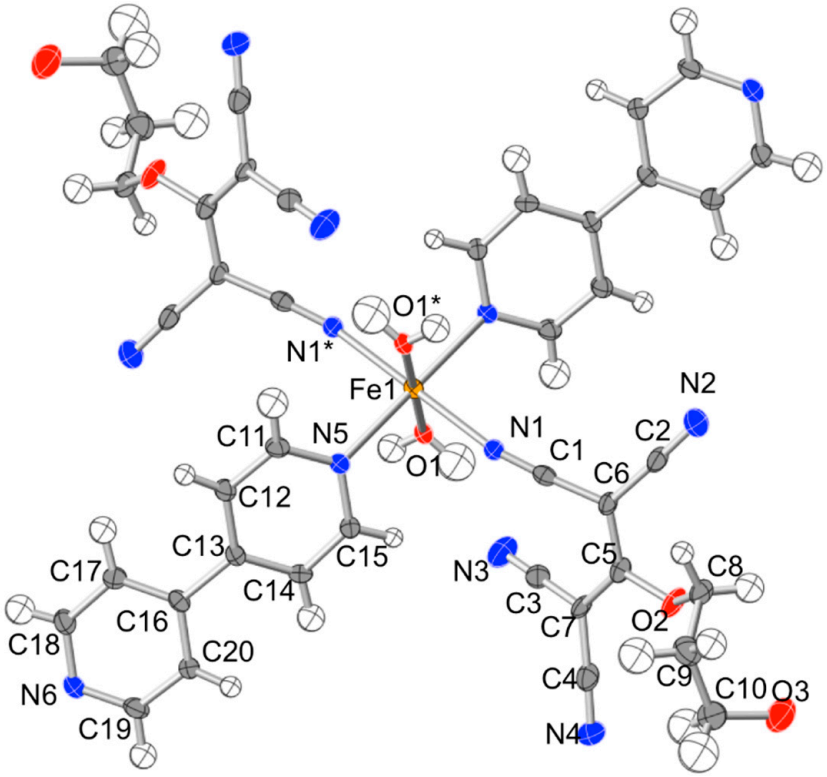

Figure 1. Structure of Compound **1** showing the labelling scheme.

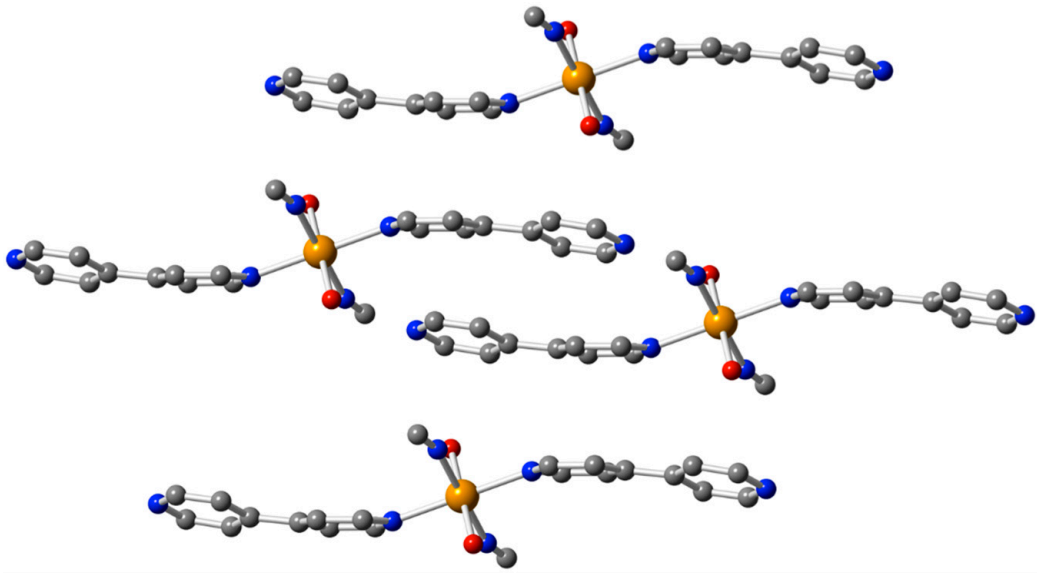

Figure 2. Crystal packing of the $[Fe(4,4'\text{-bpy})_2(\text{tcnopr3OH})_2(H_2O)_2]$ complex in **1** showing the π-π intermolecular interactions along the *a* axis.

Table 1. Main bond distances (Å) and angles (°) in Compounds **1**–**3**.

Compound	Atoms	Distance (Å)	Atoms	Angle (°)
1	Fe–N1	2.182(2)	O1–Fe–N1	90.77(7)
	Fe–N5	2.213(2)	O1–Fe–N5	90.15(6)
	Fe–O1	2.089(2)	N1–Fe–N5	91.46(7)
2	Mn1–N1	2.083(2)	N10–Mn1–N9	180
	Mn1–N5	2.109(2)	N5–Mn1–N9	89.10(5)
	Mn1–N9	2.180(2)	N1–Mn1–N10	88.36(5)
	Mn1–N10	2.140(2)	N1–Mn1–N5	91.14(8)
	Mn2–N11	2.150(2)	N12–Mn2–N11	180
	Mn2–N12	2.132(2)	O5–Mn2–N11	90.07(5)
	Mn2–O5	2.108(2)	O6–Mn2–N11	91.65(7)
	Mn2–O6	2.075(2)	O6–Mn2–O5	91.11(14)
3	Co1–N1	2.082(4)	N10–Co1–N9	180
	Co1–N5	2.106(4)	N5–Co1–N9	88.90(11)
	Co1–N9	2.153(5)	N1–Co1–N10	88.32(10)
	Co1–N10	2.144(5)	N1–Co1–N5	91.32(14)
	Co2–N11	2.146(5)	N12–Co2–N11	180
	Co2–N12	2.129(5)	O5–Co2–N11	90.30(11)
	Co2–O5	2.107(3)	O6–Co2–N11	89.52(11)
	Co2–O6	2.072(3)	O6–Co2–O5	91.11(14)

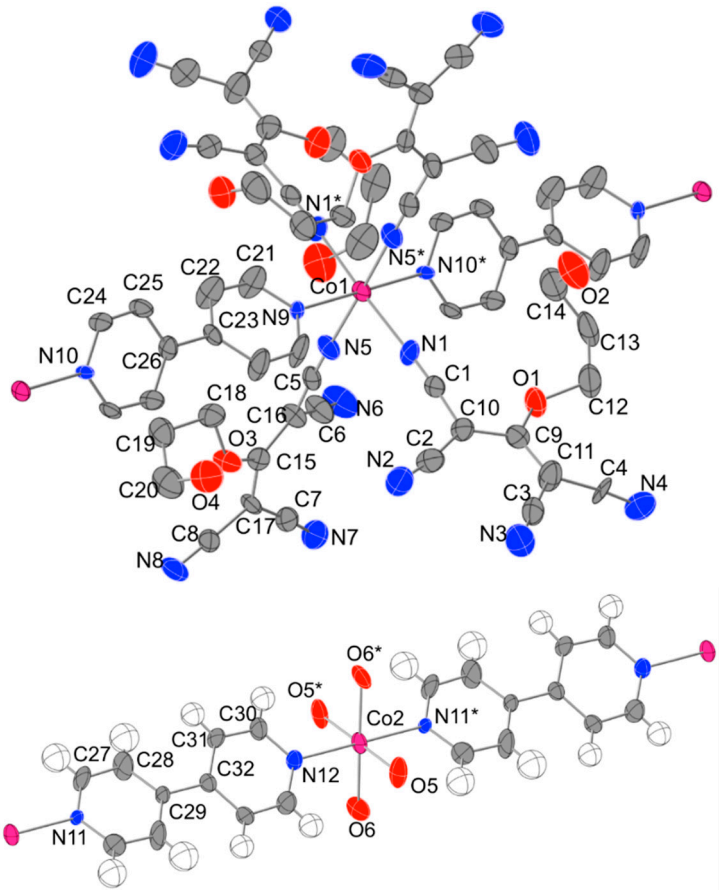

Figure 3. Structure of the anionic (top) and cationic (bottom) chains in Compound **3** showing the labelling scheme (same as in **2**).

In the cationic chain, the asymmetric unit contains one metal ion (*M*2) (Mn in **2** and Co in **3**), a 4,4′-bpy molecule, both located in a special position (3/4,−*y*,3/4) corresponding to a C_2 axis that runs along the chain axis. The asymmetric unit also contains two coordinated water molecules (O5 and O6) that become four when the C_2 axis is applied, to generate the cationic chain formulated as $[M(H_2O)_4(\mu\text{-}4,4'\text{-bpy})]^{2+}$. The asymmetric unit of the anionic chain is similar to that of the cationic one, but the water molecules are now replaced by $(tcnopr3OH)^-$ ligands, and the metal ions are labelled as *M*1. Both chains are parallel, run along the *b* axis and show a chessboard-like disposition, where each cationic chain is surrounded by four anionic chains and *vice versa* (Figure 4).

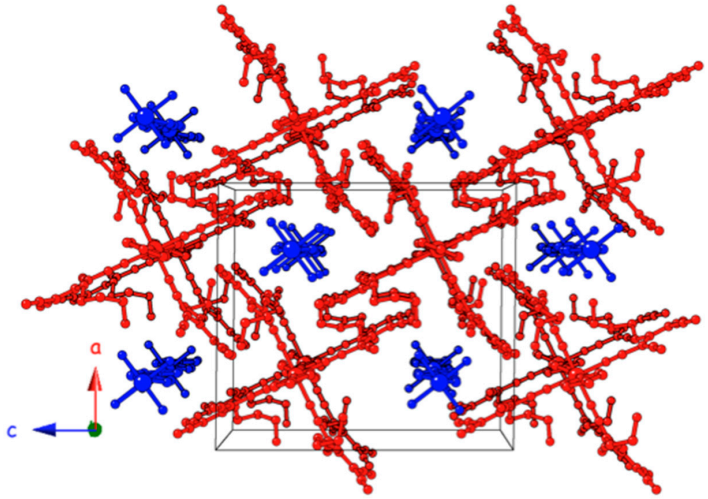

Figure 4. Perspective view of the crystal packing of Compound **3** showing the chessboard disposition of the anionic (in red) and cationic chains (in blue).

The bond distances and angles (Table 1) show that the coordination geometry of both metal atoms is octahedral, of the type N_6 for *M*1 and N_2O_4 for *M*2. *M*1 is surrounded by two N atoms from two equivalent 4,4′-bpy bridges (N11 and N12*) and four oxygen atoms from four water molecules (O5, O6 and their symmetry-related O5* and O6*; Figure 3). *M*2 is also surrounded by two N atoms from two equivalent 4,4′-bpy bridges (N9 and N1O*) and four nitrogen atoms from four $tcnopr3OH^-$ ligands (N1, N5 and their symmetry-related N1* and N5*; Figure 3).

As can be seen in Table 1, the *M*–O bond distances are shorter than the *M*–N ones, in agreement with the smaller size of the oxygen atom. In both compounds, the *M*–N bond distances for the $tcnopr3OH^-$ ligands are longer than for the 4,4′-bpy ligands, probably due to the larger steric effect of the bulky $tcnopr3OH^-$ ligands. The Mn–O and Mn–N bond distances are larger than the corresponding Co–O and Co–N, in agreement with the larger size of the Mn(II) ion.

A deeper analysis of the *M*–O and *M*–N bond distances shows that the average Mn–O bond distances are only 0.4 pm longer than the corresponding average Co–O bond distances. The same difference is observed between the average $Mn–N_{bpy}$ and $Co–N_{bpy}$ bond distances. Finally, the difference between the average $Mn–N_{tcnoprOH}$ bond distances and the corresponding $Co–N_{tcnoprOH}$ ones is 0.75 pm. Even if the standard deviations are *ca.* 0.4–0.5 pm, we can conclude that Mn(II) is only *ca.* 0.5–1.0 pm larger than Co(II). This low value contrasts with the calculated one (8.5 pm) from the ionic radii of both divalent high spin ions in an octahedral environment (Co(II) = 88.5, Mn(II) = 97 pm) [30]. Since the magnetic measurements show that in Compound **3**, the Co(II) ions are in the high spin configuration (see below), these bond differences suggest that one of the two Mn(II) ions may be in the low spin configuration (whose ionic radius is only 81 pm). If we assume that one of the Mn(II) ions is in a low spin and the other is in a high spin configuration, then the calculated difference between the average Mn–O/N and Co–O/N bond distances is 0.5 pm, in agreement with the observed value. This observation fully agrees with the magnetic measurements (see below).

Note that the Mn1–N_{bpy} bond distances are slightly longer than those of Mn_2–N_{bpy}, but this fact must be attributed to the huge steric effect of the polynitrile ligand in the anionic chain. This effect prevents a clear comparison between both Mn(II) centers from the Mn–N_{bpy} bond lengths.

2.3. Magnetic Properties

The product of the magnetic susceptibility times the temperature ($\chi_m T$) per Fe(II) atom for Compound **1** shows a value at room temperature of *ca.* 3.1 $cm^3 \cdot K \cdot mol^{-1}$, close to the expected value for an isolated $S = 2$ high spin Fe(II) with $g \approx 2$. When the sample is cooled, $\chi_m T$ remains constant down to *ca.* 30 K and shows a progressive decrease at lower temperatures to reach a value of *ca.* 1.7 $cm^3 \cdot K \cdot mol^{-1}$ at 2 K (Figure 5). Since Compound **1** presents isolated Fe(II) monomers, we have fit the magnetic data to a simple model for an $S = 2$ monomer with a zero field splitting [31], responsible for the decrease in $\chi_m T$ at low temperatures. This model reproduces very satisfactorily the magnetic properties in the whole temperature range with $g = 2.033(1)$ and $|D| = 5.7(1)$, $K = 4.0(1)$ cm^{-1} (solid line in Figure 5). This value is within the normal range found for other Fe(II) complexes [32] and may include a weak antiferromagnetic interaction through the π-π interactions observed between the Fe(II) monomers. Note that the sign of D cannot be determined from powder susceptibility measurements.

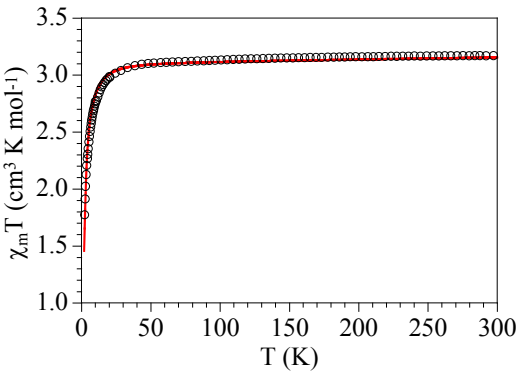

Figure 5. Thermal variation of $\chi_m T$ per Fe(II) ion for Compound **1**. The solid line is the best fit to the model (see the text).

The isothermal magnetization at 2 K shows a saturation value of *ca.* 3 μ_B, below the expected one for an isolated $S = 2$ Fe(II) ion (4 m_B) due to the presence of the zero field splitting ZFS (Figure 6). In fact, the magnetization can be well reproduced with a Brillouin function for an $S = 2$, although with a lower g value due to the ZFS (solid line in Figure 6).

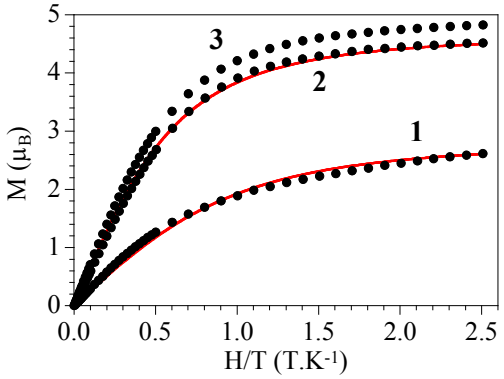

Figure 6. Isothermal magnetization at 2 K for Compounds **1**–**3** for one Fe(II) in **1** and two metal atoms in **2** and **3**. Solid lines are the best fits to the corresponding Brillouin functions (see the text).

The $\chi_m T$ product for Compound **2** shows a room temperature value of *ca.* 6.2 $cm^3 \cdot K \cdot mol^{-1}$ (Figure 7). This value is well below the expected one for two high spin (HS) $S = 5/2$ Mn(II) ions with $g = 2$ (8.75 $cm^3 \cdot K \cdot mol^{-1}$), suggesting that there is an important fraction of Mn(II) ions in the low spin (LS) configuration (in agreement with the Mn–O and Mn–N bond distances; see above). When the sample is cooled from 300 to 2 K (blue Line 1 in Figure 7), $\chi_m T$ smoothly decreases to reach a value of *ca.* 3.6 $cm^3 \cdot K \cdot mol^{-1}$ at 2 K. When the sample is heated to 400 K (red Line 2 in Figure 7), the $\chi_m T$ value increases to *ca.* 7.0 $cm^3 \cdot K \cdot mol^{-1}$. The second cooling scan from 400 to 2 K (light blue Line 3 in Figure 7) shows a smooth decrease of $\chi_m T$, although with values well above the observed ones in the heating scan. At *ca.* 70 K, both scans converge, and at lower temperatures (*ca.* 5–10 K), $\chi_m T$ reaches a plateau at a value of *ca.* 4.05 $cm^3 \cdot K \cdot mol^{-1}$, close to the expected value for an HS Mn(II) ion. Finally, at very low temperatures, $\chi_m T$ shows a more abrupt decrease, suggesting the presence of a ZFS in the HS Mn(II) ion, reaching a value of *ca.* 3.6 $cm^3 \cdot K \cdot mol^{-1}$ at 2 K. The last heating scan (orange Line 4 in Figure 7) is identical to the first one.

This behavior indicates that at 300 K, we have one Mn(II) with the HS configuration (whose $\chi_m T$ contribution is 4.375 $cm^3 \cdot K \cdot mol^{-1}$ for $g = 2$), whereas the second Mn(II) ion is mainly in the LS configuration, although there is a non-negligible fraction in the HS one. Since low spin $S = 1/2$ Mn(II) ions have a $^2T_{2g}$ ground level and present an orbital contribution, the expected $\chi_m T$ value is *ca.* 0.4–0.6 $cm^3 \cdot K \cdot mol^{-1}$. With this value, we can estimate that at 300 K, Mn2 (in the cationic chain) is in the HS configuration, whereas Mn1 (in the anionic chain) presents a mixture with *ca.* 75% in the LS configuration and *ca.* 25% in the HS one. The increase in $\chi_m T$ observed when heating the sample from 300–400 K has to be attributed to a spin crossover of the LS fraction. Although the increase of $\chi_m T$ is very smooth, the inflexion point could be located at *ca.* 370 K. From the $\chi_m T$ value at 400 K, we can estimate an HS fraction of *ca.* 60%, *i.e.*, from 300–400 K, the HS fraction has increased from *ca.* 25%–*ca.* 60% (Figure 7). The continuous decrease of $\chi_m T$ observed when cooling the sample may be attributed to: (i) the spin-orbit coupling in the LS Mn(II) fraction; (ii) to the ZFS present in the HS Mn(II) centers; and/or (iii) to a continuous and smooth SCO of the HS fraction present in the anionic chain. In fact, the thermal variation of the derivative of $\chi_m T$ for the cooling scan from 400 to 2 K shows a rounded maximum at *ca.* 50 K, suggesting that the HS to LS SCO transition is quite smooth and takes place at around 50 K (inset in Figure 7).

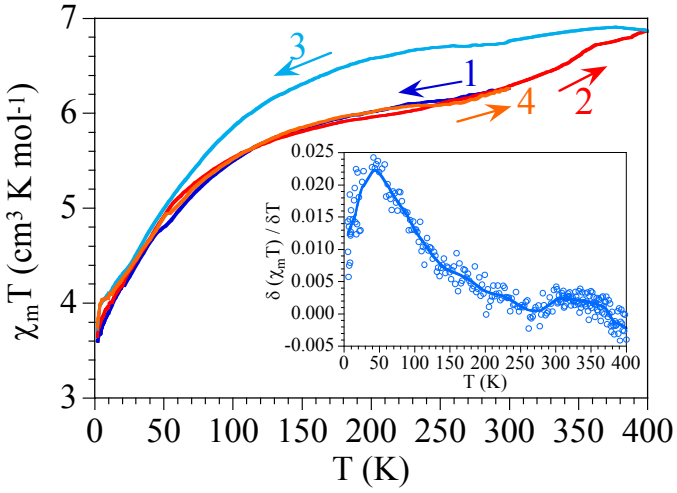

Figure 7. Thermal variation of $\chi_m T$ per formula unit for Compound **2** in two consecutive cooling and warming scans. Numbers indicate the order of the cooling and warming scans. Inset: thermal variation of the derivative of $\chi_m T$. The solid line is a 10% weighted fit.

The assignation of the LS centers to the anionic chain (where Mn1 is surrounded by four –CN groups from four tcnopr3OH$^-$ ligands) is straightforward, since the ligand field of these –CN groups

is expected to be much larger than the one created by the four water molecules coordinated to Mn2 in the cationic chain. The presence of Mn(II) in the LS configuration is very unusual. In fact, there are very few LS Mn(II) complexes, and as far as we know, this is the first time that it has been observed in a chain. In these very few examples of LS Mn(II) complexes, the metal is surrounded by a N-rich chromophore with N atoms mainly arising from cyano or oxime groups. Examples of chromophores include N_3O_3 [33], N_4S_2 [34], N_4O_2 [35] and N_6 [36–39], including six –CN groups [40,41].

Since the crystal field must be close to the thermal energy of the LS Mn(II) ions at room temperature, it is not surprising that heating the sample to 400 K leads to a partial spin crossover of the LS fraction, resulting in an increase of the HS fraction from *ca.* 25%–*ca.* 60% between 300 and 400 K. Again, this behavior is very rare, since there are very few Mn(II) complexes showing SCO [42–44], and as far as we know, although partial, this is the first time it has been observed in a Mn(II) chain.

The presence of a smooth transition with a large hysteresis suggests that the SCO transition in **2** is a kinetic process. This kind of incomplete and smooth SCO transition is typical of chain compounds, since when the metallic centers are connected, the transition of one of them exerts a chemical pressure on the bridging ligands that hampers the transition of the neighboring metal centers [45–47].

The isothermal magnetization at 2 K shows a saturation value slightly below 5 μ_B, the expected value for an HS Mn(II) ion, confirming the presence of one HS and one LS Mn(II) ion per formula unit at 2 K (Figure 6). In fact, the magnetization can be fit to a Brillouin function for an $S = 5/2$ ion, although with a reduced g value due to the presence of ZFS in the HS Mn(II) ion (solid line in Figure 6). Note that at very low temperatures, the contribution of the LS Mn(II) ions of the anionic chain must be almost negligible given the expected decrease of the magnetic moment due to the spin-orbit coupling.

Compound **3** shows a room temperature $\chi_m T$ value of *ca.* 3.2 $cm^3 \cdot K \cdot mol^{-1}$ per Co(II) ion, a value within the normal range (2.8–3.4 $cm^3 \cdot K \cdot mol^{-1}$) observed in octahedral monomeric isolated Co(II) complexes [22,48–53] These values are higher than the spin-only contribution of an $S = 3/2$ ion (1.875 $cm^3 \cdot K \cdot mol^{-1}$) due to the orbital contribution of the $^4T_{1g}$ ground state of octahedral high spin Co(II) ions. When the sample is cooled, $\chi_m T$ shows a smooth decrease due to the first-order spin orbit coupling arising from the $^4T_{1g}$ ground state. Below *ca.* 5 K, the sample shows a more abrupt decrease due to a ZFS of the Co(II) ion (Figure 8). This behavior shows that the Co(II) ions are well isolated in Compound **3**, in agreement with the structural data that show that the only bridge connecting the Co(II) is the long 4,4′-bpy.

The isothermal magnetization of Compound **3** shows a saturation value of *ca.* 4.8 μ_B for two Co(II) ions, *i.e.*, 2.4 μ_B per Co(II) ion (Figure 6). This is below the expected one for an $S = 3/2$ ground spin state (3 μ_B), since at 2 K, only the lowest Kramer's doublet is populated, giving rise to an effective $S = 1/2$ spin state. With this $S = 1/2$ spin state, the deduced effective g value is *ca.* 4.8, close to those observed in other isolated HS Co(II) complexes [22,48–53].

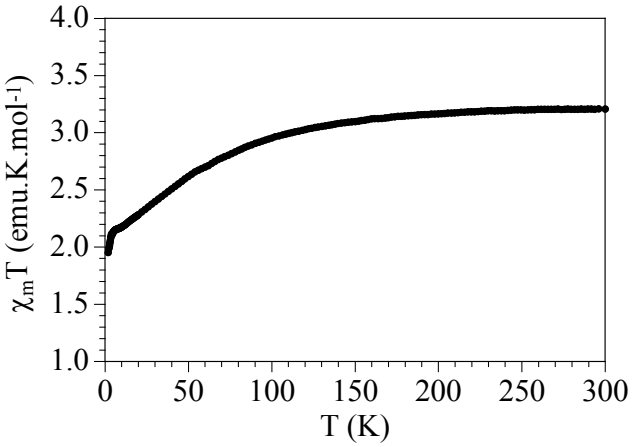

Figure 8. Thermal variation of $\chi_m T$ per Co(II) ion for Compound **3**.

2.4. Differential Scanning Calorimetry

In order to confirm the presence of a smooth partial SCO transition in the Mn(II) compound (**3**), we have performed differential scanning calorimetric measurements on Compound **3** (Figure 9).

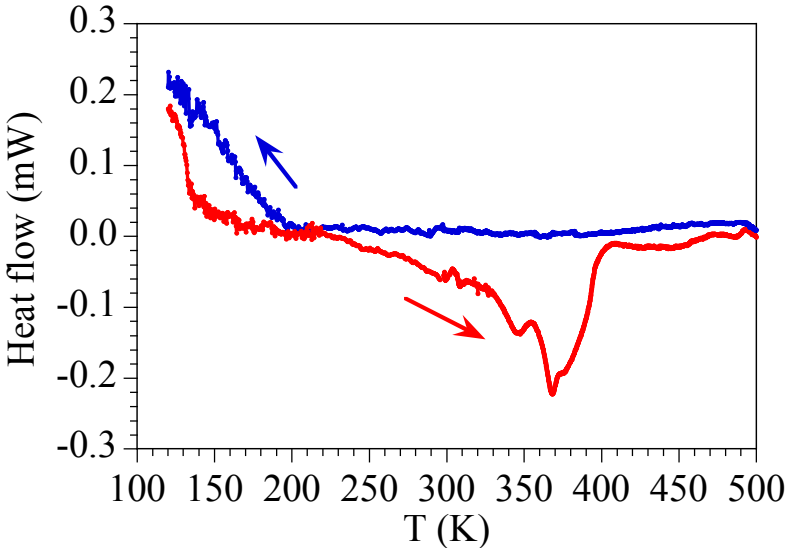

Figure 9. Differential scanning calorimetric measurements for Compound **3** in the heating (red) and cooling (blue) scans.

These measurements show a large exothermic peak in the heating scan at *ca.* 370 K and a smaller one at *ca.* 350 K corresponding to the smooth SCO transition of the Mn(II) ions of the anionic chain observed at the same temperatures in the magnetic measurements. In the cooling scan, the SCO transition is observed with a very large peak centered below 120 K, precluding a clear observation of the maximum. This large peak confirms the reversibility of the SCO and the large hysteresis observed in the magnetic measurements and suggests that the decrease observed in the magnetic moment on cooling the sample is due to a gradual and smooth SCO of the Mn(II) centers. Unfortunately, since the SCO transition is very smooth and is only partial, it is very hard to obtain reliable values of the transition temperatures in the hysteresis loop from DSC measurements.

3. Experimental Section

3.1. Starting Materials

The reagents 4,4′-bipyridine, $FeCl_2 \cdot 4H_2O$, $MnCl_2 \cdot 4H_2O$ and $CoCl_2 \cdot 6H_2O$ are commercial and were used as received.

3.2. Synthesis of the 1,1,3,3-Tetracyano-2-(3-hydroxypropoxy)-propenide (tcnopr3OH$^-$) Ligand

The potassium salt of the 1,1,3,3-tetracyano-2-(3-hydroxypropoxy)-propenide, K[tcnopr3OH], ligand was prepared following the reported method [25].

*3.3. Synthesis of Compound [Fe^{II}(tcnopr3OH)$_2$(H_2O)$_2$(4,4′-bpy)$_2$] (**1**)*

An aqueous solution (9 mL) of K[tcnopr3OH] (250 mg, 1 mmol) was added with stirring to an aqueous solution (2 mL) of $FeCl_2 \cdot 4H_2O$ (99 mg, 0.5 mmol). An ethanolic solution (15.6 mL) of 4,4′-bipyridine (78 mg, 0.5 mmol) was added with stirring to the resulting solution, and the final solution was filtered. Slow evaporation of the filtrate at room temperature afforded amber single crystals of **1** suitable for X-ray structure determination. IR data (n, cm^{-1}): 3455 m, 3320 br, 2196 s,

1610 w, 1508 w, 1485 s, 1415 m, 1347 m, 1171 m, 1044 m. Anal. calcd. for $C_{40}H_{34}FeN_8O_6$ (778.58): C 61.70, H 4.40, N 14.39; found: C 61.20, H 4.34, N 14.27.

*3.4. Synthesis of [M(H$_2$O)$_4$(μ-4,4′-bpy)][M(tcnoprOH)$_4$(μ-4,4′-bpy)].3H$_2$O (M^{II} = Mn (**2**) and Co (**3**))*

Compounds **2** and **3** were prepared using a similar method to **1**, but using $MnCl_2 \cdot 4H_2O$ (99 mg, 0.5 mmol) for **2** and $CoCl_2 \cdot 6H_2O$ (119 mg, 0.5 mmol) for **3**. Slow evaporation of the filtrates at room temperature afforded lilac and orange single crystals of **2** and **3**, respectively, suitable for X-ray structure determination. Anal. calcd. for **2**: $C_{60}H_{58}Mn_2N_{20}O_{15}$ (1409.14): C 51.14, H 4.15, N 19.88; found: C 51.20, H 4.04, N 19.77. Anal. calcd. for **3**: $C_{60}H_{58}Co_2N_{20}O_{15}$ (1417.12): C 50.85, H 4.13, N 19.77; found: C 50.60, H 4.03, N 19.57. IR data for **2** (ν, cm^{-1}): 3400 m, 3337 br, 2202 s, 1605 w, 1490 s, 1420 m, 1398 m, 1377 m, 1174 m, 1076 m. IR data for **3** (ν, cm^{-1}): 3440 m, 3311 br, 2244 m, 2199 s, 1736 s, 1720 s, 1609 w, 1497 s, 1460 m, 1398 m, 1346 m, 1150 m, 1068 m.

3.5. Physical Measurements

IR spectra (4000–400 cm^{-1}) were recorded with a Nexus Nicolet (Madison, WI, USA) FT-IR spectrophotometer in KBr pellets. DSC measurements were carried out on a Mettler Toledo (Leicester, UK) DSC 821e over the range 120–500 K with a scan rate of 5 K/min in N_2.

The magnetic susceptibility measurements were carried out in the temperature range 2–300 K (2–400 K for **2**) with an applied magnetic field of 0.1 T on polycrystalline samples of Compounds **1**–**3** (with masses of 37.64, 19.27 and 31.75 mg, respectively) with a Quantum Design (San Diego, CA, USA) MPMS-XL-5 SQUID susceptometer. The isothermal magnetizations were performed on the same samples at 2 K with magnetic fields up to 5 T. The susceptibility data were corrected for the sample holders previously measured using the same conditions and for the diamagnetic contributions of the salt as deduced by using Pascal's constant tables ($\chi_{dia} = -422.9 \times 10^{-6}$, -734.5×10^{-6} and -727.3×10^{-6} emu·mol^{-1} for **1**–**3**, respectively) [54].

3.6. Crystallographic Data Collection and Refinement

Suitable single crystals of Compounds **1**–**3** were mounted on glass fibers using a viscous hydrocarbon oil to coat the crystals and then transferred directly to the cold nitrogen stream for data collection. X-ray data were collected at 170 K (for **1**) and 120 K (for **2**) on a Supernova diffractometer equipped with a graphite-monochromated Enhance (Mo) X-ray Source (λ = 0.71073 Å). For Compound **3,** X-ray crystal data were collected at 170 K on an Oxford-Diffraction Xcalibur CCD diffractometer equipped with a graphite-monochromated (Mo) X-ray source (λ = 0.71073 Å). The program CrysAlisPro, Oxford Diffraction Ltd., was used for unit cell determinations and data reduction [55]. Empirical absorption correction was performed using spherical harmonics, implemented in the SCALE3 ABSPACK scaling algorithm. The structures were solved by direct methods and successive Fourier difference syntheses and refined on F^2 by weighted anisotropic full-matrix least-squares methods [56]. All non-hydrogen atoms were refined anisotropically, and all of the hydrogen atoms were located by a difference Fourier map and then refined isotropically for all compounds. Scattering factors and corrections for anomalous dispersion were taken from the International Tables for X-ray Crystallography [57]. Data collection and data reduction were done with the CRYSALIS-CCD and CRYSALIS-RED programs [58,59] All of the other calculations were done with WinGX [60]. Data collection and refinement parameters are given in Table 2. CCDC-1442430 (**1**), CCDC-1442431 (**2**) and CCDC-1442432 (**3**) contain the supplementary crystallographic data for this paper. These data can be obtained free of charge from The Cambridge Crystallographic Data Centre via www.ccdc.cam.ac.uk/data_request/cif.

Table 2. Crystal data and structure refinement of Complexes **1**–**3**.

Compound	1	2	3
Formula	$C_{40}H_{34}FeN_8O_6$	$C_{60}H_{58}Mn_2N_{20}O_{15}$	$C_{60}H_{58}Co_2N_{20}O_{15}$
F. Wt.	778.58	1409.14	1417.12
Crystal system	Triclinic	Monoclinic	Monoclinic
Space group	*P-1*	*P2/n*	*P2/n*
a (Å)	8.4903(2)	16.1494(4)	16.2245(8)
b (Å)	9.4790(4)	11.3855(2)	11.3941(4)
c (Å)	12.3652(5)	18.0358(4)	18.0389(8)
α (°)	93.553(1)	90.00	90.00
β (°)	105.405(3)	90.594(2)	90.693(5)
γ (°)	91.720(3)	90.00	90.00
V (Å^3)	956.43(6)	3316.05(12)	3334.5(3)
Z	2	2	2
T (K)	170	120	170
ρ_{calc} (g.cm^{-3})	1.449	1.411	1.411
μ (cm^{-1})	0.460	0.461	0.577
F(000)	432	1456	1464
q range (°)	2.85–25.40	2.26–32.68	2.88–26.94
Total reflections	5153	126001	21361
Unique reflections	2339	11694	5381
R_{int}	0.0205	0.0899	0.0808
Data with $I > 2\sigma(I)$	1878	5479	2116
N_v	336	469	469
[a] *R1*	0.029	0.0473	0.0441
[b] *wR2*	0.0688	0.1341	0.1142
[c] GooF	1.000	0.867	0.875
$\Delta\rho_{max,min}$ (eÅ^{-3})	+0.263	+0.887	+0.360
$\Delta\rho_{max,min}$ (eÅ^{-3})	−0.197	−0.577	−0.213

[a] $R1 = \sum |Fo\text{-}Fc| / Fo$; [b] $wR2 = \{S[w(F_o^2 - F_c^2)^2] / S[w(F_o^2)^2]\}^{1/2}$; [c] $GooF = \{S[w(F_o^2 - F_c^2)^2] / (N_{obs} - N_{var})\}^{1/2}$.

4. Conclusions

The use of the polynitrile ligand tcnopr3OH$^-$ with a bridging co-ligand as 4,4′-bpy has given rise to three novel compounds with Fe(II), Mn(II) and Co(II). The Fe(II) ion has yielded an unexpected monomer, where the Fe(II) ion is located on an inversion center and is surrounded by two *trans* tcnopr3OH$^-$ ligands, two *trans* 4,4′-bpy terminal ligands and two *trans* water molecules. Interestingly, for Mn(II) and Co(II), the complexes formed present segregated cationic and anionic chains. In the cationic chains, formulated as $[M(4,4'\text{-bpy})(H_2O)_4]^{2+}$, the *M* atoms are surrounded by two *trans* bridging 4,4′-bpy ligands and four water molecules, whereas in the anionic chains, formulated as $[M(4,4'\text{-bpy})(\text{tcnopr3OH})_4]^{2-}$, the *M* atoms are surrounded by two *trans* bridging 4,4′-bpy ligands and four tcnopr3OH ligands. The Mn(II) compound is very original, since it presents HS Mn(II) centers (in the cationic chain) coexisting with LS Mn(II) centers (*ca.* 75% of the Mn(II) centers in the anionic chain). Furthermore, these LS Mn(II) centers show an even more unusual spin crossover (SCO) transition implying *ca.* 45% of the LS centers from 300–400 K. As far as we know, this is the first Mn(II) chain compound presenting an LS configuration, the first example of the coexistence of HS and LS Mn(II) centers in the same compound and the first example of SCO in a Mn(II) chain compound. This surprising result has been confirmed by DSC measurements, which confirm the presence of the smooth SCO transition and its reversibility.

Acknowledgments: We thank the Spanish MINECO (Projects CTQ2011-26507, CTQ2014-52758-P and MAT2014-56143-R) and the Generalitat Valenciana (Projects PrometeoII/2014/076, GVACOMP2015-246 and ISIC) for financial support.

Author Contributions: S.B. participated in the preparations, characterizations and X-ray structural analysis. S.T. participated in the X-ray structure analysis. C.J.G.G. performed the magnetic and DSC measurements, analyzed the data and wrote the manuscript.

Conflicts of Interest: The authors declare no conflict of interest.

References

1. Huang, Y.; Jiang, F.; Hong, M. Magnetic lanthanide–transition-Metal organic–inorganic Hybrid Materials: From Discrete Clusters to Extended Frameworks. *Coord. Chem. Rev.* **2009**, *253*, 2814–2834. [CrossRef]
2. Weng, D.; Wang, Z.; Gao, S. Framework-Structured Weak Ferromagnets. *Chem. Soc. Rev.* **2011**, *40*, 3157–3181. [CrossRef] [PubMed]
3. Atzori, M.; Benmansour, S.; Espallargas, G.M.; Clemente-León, M.; Abhervé, A.; Gómez-Claramunt, P.; Coronado, E.; Artizzu, F.; Sessini, E.; Deplano, P.; *et al*. A Family of Layered Chiral Porous Magnets Exhibiting Tunable Ordering Temperatures. *Inorg. Chem.* **2013**, *52*, 10031–10040. [CrossRef] [PubMed]
4. Givaja, G.; Amo-Ochoa, P.; Gómez-García, C.J.; Zamora, F. Electrical Conductive Coordination Polymers. *Chem. Soc. Rev.* **2012**, *41*, 115–147. [CrossRef] [PubMed]
5. Allendorf, M.D.; Bauer, C.A.; Bhakta, R.K.; Houk, R.J.T. Luminescent Metal-Organic Frameworks. *Chem. Soc. Rev.* **2009**, *38*, 1330–1352. [CrossRef] [PubMed]
6. Rocha, J.; Carlos, L.D.; Paz, F.A.A.; Ananias, D. Luminescent Multifunctional Lanthanides-Based Metal-Organic Frameworks. *Chem. Soc. Rev.* **2011**, *40*, 926–940. [CrossRef] [PubMed]
7. Bhowmik, P.; Biswas, S.; Chattopadhyay, S.; Diaz, C.; Gómez-García, C.J.; Ghosh, A. Synthesis, Crystal Structure and Magnetic Properties of Two Alternating Double $\mu_{1,1}$ and $\mu_{1,3}$ Azido Bridged Cu(II) and Ni(II) Chains. *Dalton Trans.* **2014**, *43*, 12414–12421. [CrossRef] [PubMed]
8. Adhikary, C.; Koner, S. Structural and Magnetic Studies on Copper(II) Azido Complexes. *Coord. Chem. Rev.* **2010**, *254*, 2933–2958. [CrossRef]
9. Escuer, A.; Aromí, G. Azide as a Bridging Ligand and Magnetic Coupler in Transition Metal Clusters. *Eur. J. Inorg. Chem.* **2006**, *2006*, 4721–4736. [CrossRef]
10. Escuer, A.; Esteban, J.; Perlepes, S.P.; Stamatatos, T.C. The Bridging Azido Ligand as a Central Player in High-Nuclearity 3d-Metal Cluster Chemistry. *Coord. Chem. Rev.* **2014**, *275*, 87–129. [CrossRef]
11. Gu, Z.; Zuo, J.; You, X. A Three-Dimensional Ferromagnet Based on Linked Copper-Azido Clusters. *Dalton Trans.* **2007**, 4067–4072. [CrossRef] [PubMed]
12. Newton, G.N.; Nihei, M.; Oshio, H. Cyanide-Bridged Molecular Squares? the Building Units of Prussian Blue. *Eur. J. Inorg. Chem.* **2011**, *2011*, 3031–3042. [CrossRef]
13. Biswas, S.; Gómez-García, C.J.; Clemente-Juan, J.M.; Benmansour, S.; Ghosh, A. Supramolecular 2D/3D Isomerism in a Compound Containing Heterometallic $Cu^{II}_2Co^{II}$ Nodes and Dicyanamide Bridges. *Inorg. Chem.* **2014**, *53*, 2441–2449. [CrossRef] [PubMed]
14. Turner, D.R.; Chesman, A.S.R.; Murray, K.S.; Deacon, G.B.; Batten, S.R. The Chemistry and Complexes of Small Cyano Anions. *Chem. Commun.* **2011**, *47*, 10189–10210. [CrossRef] [PubMed]
15. Batten, S.R.; Murray, K.S. Structure and Magnetism of Coordination Polymers Containing Dicyanamide and Tricyanomethanide. *Coord. Chem. Rev.* **2003**, *246*, 103–130. [CrossRef]
16. Tamaki, H.; Zhong, Z.J.; Matsumoto, N.; Kida, S.; Koikawa, M.; Achiwa, N.; Hashimoto, Y.; Okawa, H. Design of Metal-Complex Magnets. Syntheses and Magnetic Properties of Mixed-Metal Assemblies $\{NBu_4[MCr(ox)_3]\}_x$ (NBu_4^+ = Tetra(*n*-Butyl)Ammonium Ion; ox^{2-} = Oxalate Ion; M = Mn^{2+}, Fe^{2+}, Co^{2+}, Ni^{2+}, Cu^{2+}, Zn^{2+}). *J. Am. Chem. Soc.* **1992**, *114*, 6974–6979. [CrossRef]
17. Kumar, G.; Gupta, R. Molecularly Designed Architectures—The Metalloligand Way. *Chem. Soc. Rev.* **2013**, *42*, 9403–9453. [CrossRef] [PubMed]
18. Das, L.K.; Gómez-García, C.J.; Drew, M.G.B.; Ghosh, A. Playing with Different Metalloligands [NiL] and Hg to [NiL] Ratios to Tune the Nuclearity of Ni(II)-Hg(II) Complexes: Formation of *di-*, *tri-*, *hexa-* and *nona*-Nuclear Ni-Hg Clusters. *Polyhedron* **2015**, *87*, 311–320. [CrossRef]
19. Das, L.K.; Gómez-García, C.; Ghosh, A. Influence of the Central Metal Ion in Controlling the Self-Assembly and Magnetic Properties of 2D Coordination Polymers Derived from $(NiL)_2M]^{2+}$ Nodes (M = Ni, Zn and Cd) (H_2L = Salen-Type Di-Schiff Base) and Dicyanamide Spacers. *Dalton Trans.* **2015**, *44*, 1292–1302. [CrossRef] [PubMed]
20. Thetiot, F.; Triki, S.; Pala, J.S.; Gómez-García, C.J. New Coordination Polymers with a 2,2-Dicyano-1-Ethoxyethenolate ($Dcne^-$) Bridging Ligand: Syntheses, Structural Characterisation and Magnetic Properties of $[M(Dcne)_2(H_2O)_2]$ (M = Mn^{II}, Fe^{II}, Co^{II}, Ni^{II} and Zn^{II}) and $[Cu(Dcne)_2(H_2O)]$. *J. Chem. Soc. Dalton Trans.* **2002**, 1687–1693. [CrossRef]

21. Benmansour, S.; Setifi, F.; Triki, S.; Salaun, J.Y.; Vandevelde, F.; Sala-Pala, J.; Gómez-García, C.J.; Roisnel, T. New Multidimensional Coordination Polymers with μ_2- and μ_3-Dcno Cyano Carbanion Ligand {dcno$^-$ = $[(NC)_2CC(O)O(CH_2)_2OH]^-$}. *Eur. J. Inorg. Chem.* **2007**, 186–194. [CrossRef]
22. Benmansour, S.; Setifi, F.; Gómez-García, C.J.; Triki, S.; Coronado, E.; Salaun, J.Y. A Novel Polynitrile Ligand with Different Coordination Modes: Synthesis, Structure and Magnetic Properties of the Series $[M(tcnoprOH)_2(H_2O)_2]$ (M = Mn, Co and Cu) (tcnoprOH$^-$ = $[(NC)_2CC(OCH_2CH_2CH_2OH)C(CN)_2]^-$). *J. Mol. Struct.* **2008**, *890*, 255–262. [CrossRef]
23. Atmani, C.; Setifi, F.; Benmansour, S.; Triki, S.; Marchivie, M.; Salaun, J.Y.; Gómez-García, C.J. New Planar Polynitrile Dianion and its First Coordination Polymer with Unexpected Short M$\cdots$M Contacts (Tcno^{2-} = $[(NC)_2CC(O)C(CN)_2]^{2-}$). *Inorg. Chem. Commun.* **2008**, *11*, 921–924. [CrossRef]
24. Kremer, C.; Melián, C.; Torres, J.; Juanicó, M.P.; Lamas, C.; Pezaroglo, H.; Manta, E.; Schumann, H.; Pickardt, J.; Girgsdies, F.; *et al*. Synthesis, Structure and Magnetic Properties of Mn(II) and Cu(II) Complexes with the Dicyano-Acetic Acid Methyl Ester Anion. *Inorg. Chim. Acta* **2001**, *314*, 83–90. [CrossRef]
25. Thétiot, F.; Triki, S.; Pala, J.S. Polynitriles as Ligands: New Coordination Polymers with the 1,1,3,3-Tetracyano-2-Ethoxypropenide (Tcnp$^-$) Bridging Ligand. *Polyhedron* **2003**, *22*, 1837–1843. [CrossRef]
26. Triki, S.; Pala, J.S.; Decoster, M.; Molinié, P.; Toupet, L. Novel Infinite Three-Dimensional Networks with Highly Conjugated Polynitrile Ligands: Syntheses, Crystal Structures, and Magnetic Properties of $[Cu\{C[C(CN)_2]_3\}(H_2O)_2]_n$ and $[Cu\{C[C(CN)_2]_3\}(en)]_n$ (en = $NH_2CH_2CH_2NH_2$). *Angew. Chem. Int. Ed.* **1999**, *38*, 113–115. [CrossRef]
27. Benmansour, S.; Atmani, C.; Setifi, F.; Triki, S.; Marchivie, M.; Gómez-García, C.J. Polynitrile Anions as Ligands: From Magnetic Polymeric Architectures to Spin Crossover Materials. *Coord. Chem. Rev.* **2010**, *254*, 1468–1478. [CrossRef]
28. Benmansour, S.; Setifi, F.; Triki, S.; Gómez-García, C.J. Linkage Isomerism in Coordination Polymers. *Inorg. Chem.* **2012**, *51*, 2359–2365. [CrossRef] [PubMed]
29. Benmansour, S.; Setifi, F.; Gómez-García, C.J.; Triki, S.; Coronado, E. New Coordination Polymers Based on a Novel Polynitrile Ligand: Synthesis, Structure and Magnetic Properties of the Series $[M(tcnoetOH)_2(4,4'\text{-Bpy})(H_2O)_2]$ (tcnoetOH$^-$ =$[(NC)_2CC(OCH_2CH_2OH)C(CN)_2]^-$; M = Fe, Co and Ni). *Inorg. Chim. Acta* **2008**, *361*, 3856–3862. [CrossRef]
30. Shannon, R. Revised Effective Ionic Radii and Systematic Studies of Interatomic Distances in Halides and Chalcogenides. *Acta Crystallogr. A* **1976**, *32*, 751–767. [CrossRef]
31. O'Connor, C.J. Magnetochemistry-Advances in Theory and Experimentation. *Prog. Inorg. Chem.* **1982**, *29*, 203–283.
32. Boca, R. Zero-Field Splitting in Metal Complexes. *Coord. Chem. Rev.* **2004**, *248*, 757–815. [CrossRef]
33. Basu, P.; Chakravorty, A. Low-Spin Tris(Quinone Oximates) of Manganese(II,III). Synthesis, Isomerism, and Equilibria. *Inorg. Chem.* **1992**, *31*, 4980–4986. [CrossRef]
34. Karmakar, S.; Choudhury, S.; Chakravorty, A. Thioether Binding of Low-Spin Bivalent Manganese. A MS_2N_4 Family Furnished by New Hexadentate Thioether-Oxime-Azo Ligands (M = Mn^{II}, Fe^{II}, Fe^{III}). *Inorg. Chem.* **1994**, *33*, 6148–6153. [CrossRef]
35. Ganguly, S.; Karmakar, S.; Pal, C.; Chakravorty, A. Regiospecific Oximato Coordination at the Oxygen Site: Ligand Design and Low-Spin Mn and Fe Species. *Inorg. Chem.* **1999**, *38*, 5984–5987. [CrossRef] [PubMed]
36. Saha, A.; Majumdar, P.; Goswami, S. Low-Spin Manganese(II) and Cobalt(III) Complexes of N-Aryl-2-Pyridylazophenylamines: New Tridentate N,N,N-Donors Derived from Cobalt Mediated Aromatic Ring Amination of 2-(Phenylazo)Pyridine. Crystal Structure of a Manganese(II) Complex. *Dalton Trans.* **2000**, 1703–1708. [CrossRef]
37. Knof, U.; Weyhermuller, T.; Wolter, T.; Wieghardt, K. Synthesis of Low Spin $[Mn(L2)_2]I_2\cdot 2MeOH$ and [Cu(L1)] Via Condensation of S-Methylisothiosemicarbazide and Pentane-2,4-Dione in the Presence of Air. *J. Chem. Soc. Chem. Commun.* **1993**, 726–728. [CrossRef]
38. Chattopadhyay, S.; Basu, P.; Pal, S.; Chakravorty, A. Synthesis and Structure of a Trinuclear Manganese(II) Complex Containing Low-Spin Metal. *J. Chem. Soc. Dalton Trans.* **1990**, 3829–3833. [CrossRef]
39. Cotton, F.A.; Monchamp, R.; Henry, R.; Young, R. The Preparation and Properties of a New Pentacyanomanganesenitric Oxide Anion, $[Mn(CN)_5NO]^{2-}$, and some Observations on Other Pentacyanonitrosyl Complexes. *J. Inorg. Nucl. Chem.* **1959**, *10*, 28–38. [CrossRef]

40. Entley, W.R.; Girolami, G. New Three-Dimensional Ferrimagnetic Materials: $K_2Mn[Mn(CN)_6]$, $Mn_3[Mn(CN)_6]_2 \cdot 12H_2O$, and $CsMn[Mn(CN)_6] \cdot 1/2H_2O$. *Inorg. Chem.* **1994**, *33*, 5165–5166. [CrossRef]
41. Ohba, M.; Ōkawa, H. Synthesis and Magnetism of Multi-Dimensional Cyanide-Bridged Bimetallic Assemblies. *Coord. Chem. Rev.* **2000**, *198*, 313–328. [CrossRef]
42. Goodwin, H.A.; Gutlich, P. Spin Crossover in Transition Metal Compounds II Thermal Spin Crossover in Mn(II), Mn(III), Cr(II) and Co(III) Coordination Compounds. *Top. Curr. Chem.* **2004**, *234*, 49–62.
43. Scheuermayer, S.; Tuna, F.; Bodensteiner, M.; Scheer, M.; Layfield, R.A. Spin Crossover in Phosphorus- and Arsenic-Bridged Cyclopentadienyl-Manganese(II) Dimers. *Chem. Commun.* **2012**, *48*, 8087–8089. [CrossRef] [PubMed]
44. Ohkoshi, S.; Tokoro, H.; Utsunomiya, M.; Mizuno, M.; Abe, M. Observation of Spin Transition in an Octahedrally Coordinated Manganese(II) Compound. *J. Phys. Chem. B* **2002**, *106*, 2423–2425. [CrossRef]
45. Dupouy, G.; Marchivie, M.; Triki, S.; Sala-Pala, J.; Gómez-García, C.J.; Pillet, S.; Lecomte, C.; Letard, J.F. Photoinduced HS State in the First Spin-Crossover Chain Containing a Cyanocarbanion as Bridging Ligand. *Chem. Commun.* **2009**, 3404–3406. [CrossRef] [PubMed]
46. Atmani, C.; El Hajj, F.; Benmansour, S.; Marchivie, M.; Triki, S.; Conan, F.; Patinec, V.; Handel, H.; Dupouy, G.; Gómez-García, C.J. Guidelines to Design New Spin Crossover Materials. *Coord. Chem. Rev.* **2010**, *254*, 1559–1569. [CrossRef]
47. Dupouy, G.; Triki, S.; Marchivie, M.; Cosquer, N.; Gómez-García, C.J.; Pillet, S.; Bendeif, E.; Lecomte, C.; Asthana, S.; Létard, J.F. Cyanocarbanion-Based Spin-Crossover Materials: Photocrystallographic and Photomagnetic Studies of a New Iron(II) Neutral Chain. *Inorg. Chem.* **2010**, *49*, 9358–9368. [CrossRef] [PubMed]
48. Shi, Z.Y.; Peng, J.; Gómez-García, C.J.; Benmansour, S.; Gu, X.J. Influence of Metal Ions on the Structures of Keggin Polyoxometalate-Based Solids: Hydrothermal Syntheses, Crystal Structures and Magnetic Properties. *J. Solid State Chem.* **2006**, *179*, 253–265. [CrossRef]
49. Humphrey, S.M.; Alberola, A.; Gómez-García, C.J.; Wood, P.T. A New Co(II) Coordination Solid with Mixed Oxygen, Carboxylate, Pyridine and Thiolate Donors Exhibiting Canted Antiferromagnetism with $T_C \approx 68$ K. *Chem. Commun.* **2006**, 1607–1609. [CrossRef] [PubMed]
50. Gómez-García, C.J.; Coronado, E.; Borrás-Almenar, J.J. Magnetic Characterization of Tetranuclear Copper(II) and Cobalt(II) Exchange-Coupled Clusters Encapsulated in Heteropolyoxotungstate Complexes. Study of the Nature of the Ground States. *Inorg. Chem.* **1992**, *31*, 1667–1673. [CrossRef]
51. Liu, H.S.; Gómez-García, C.J.; Peng, J.; Sha, J.Q.; Wang, L.X.; Yan, Y.C. A Co-Monosubstituted Keggin Polyoxometalate with an Antenna Ligand and Three Cobalt(II) Chains as Counterion. *Inorg. Chim. Acta* **2009**, *362*, 1957–1962. [CrossRef]
52. Lloret, F.; Julve, M.; Cano, J.; Ruiz-García, R.; Pardo, E. Magnetic Properties of Six-Coordinated High-Spin Cobalt(II) Complexes: Theoretical Background and its Application. *Inorg. Chim. Acta* **2008**, *361*, 3432–3445. [CrossRef]
53. Mosconi, E.; Yum, J.; Kessler, F.; Gómez García, C.J.; Zuccaccia, C.; Cinti, A.; Nazeeruddin, M.K.; Grätzel, M.; de Angelis, F. Cobalt electrolyte/dye Interactions in Dye-Sensitized Solar Cells: A Combined Computational and Experimental Study. *J. Am. Chem. Soc.* **2012**, *134*, 19438–19453. [CrossRef] [PubMed]
54. Bain, G.A.; Berry, J.F. Diamagnetic Corrections and Pascal's Constants. *J. Chem. Educ.* **2008**, *85*, 532–536. [CrossRef]
55. CrysAlisPro, Version 171.33.55. Oxford Diffraction Ltd. Oxford, UK, 2004.
56. Sheldrick, M. *SHELX97: Programs for Crystal Structure Analysis*; University of Göttingen: Göttingen, Germany, 1997.
57. *International Tables for X-ray Crystallography*; Kyn och Press: Birmingham, UK, 1975.
58. Crysalis-Ccd, Version 170. Oxford Diffraction Ltd. Oxford, UK, 2002.
59. Crysalis-Red, Version 170. Oxford Diffraction Ltd. Oxford, UK, 2002.
60. Farrugia, L.J. WinGX Suite for Small-Molecule Single-Crystal Crystallography. *J. Appl. Cryst.* **1999**, *32*, 837–838. [CrossRef]